Check for updates

ADVANCED SUSTAINABLE SYSTEMS
www.advsustainsys.com

Strong Metal-Support Interaction-Induced Regulation of Hydrogen Adsorption Behavior of Uniform Ru Nanoparticles Integrated with CoP Nanosheets for High-Efficiency Electrochemical Hydrogen Production

Yufeng Zhu, Jing Li, Guangyao Zhou, Leiming Qian, Yu Fang, Mingjiang Xu, Huan Pang, Mingyi Zhang, Jianping Xu, Jun Yang,* Lin Xu,* and Yawen Tang**

The ingenious modification of the hydrogen adsorption state of ruthenium (Ru) for achieving high-efficiency electrocatalytic performance is of vital importance for water electrolysis technology. Herein, a novel heterostructured catalyst composed of highly dispersed ultrafine Ru nanoparticles immobilized on CoP nanosheet (denoted as Ru/CoP hereafter) is developed through a feasible "impregnation-phosphorization" strategy. Experimental results and density functional theory (DFT) simulations collectively indicate that the strong metal-support interaction (SMSI) effect between Ru nanoparticles and CoP nanosheet substrate can dramatically tailor the electronic configurations of active centers, thus accelerating the charge transfer rate and regulating the hydrogen binding energy. Consequently, the Ru/CoP electrocatalyst with optimal Ru loading content demonstrates prominent HER performance in alkaline solution with a low overpotential of 36 mV to afford a current density of 10 mA cm^{-2} and a small Tafel slope of 73.0 mV dec^{-1}, which can almost compete with that of commercial Pt/C. This work provides a new inspiration for the elaborate modification of intermediate adsorption capacity and enhancement of electrocatalytic performance for high-efficiency electrocatalysts in energy conversion fields.

1. Introduction

A serious global energy crisis and greenhouse effect resulting from the consumption of a large amount of traditional fossil energy have stimulated the extensive of clean and sustainable energy sources.[1] Thanks to the high energy density and zero carbon emission features, hydrogen (H_2) has been deemed as one of the most promising candidates to replace fossil fuels in the future ecological society.[2] Among various hydrogen production methods, electrocatalytic hydrogen evolution reaction (HER) is considered as one of the most potential hydrogen production methods profiting from the advantages of eco-friendliness and high-purity hydrogen.[3] Up to now, noble Pt-based materials still represent the most ideal electrocatalysts for HER, whereas the scarce reserves and high cost impede their large-scale

Y. Zhu, J. Li, L. Qian, Y. Fang, M. Xu, L. Xu, Y. Tang
School of Chemistry and Materials Science
Nanjing Normal University
Nanjing 210023, China
E-mail: xulin001@njnu.edu.cn; tangyawen@njnu.edu.cn

G. Zhou
College of Science
Jinling Institute of Technology
Nanjing 211169, P. R. China
E-mail: zhouguangyao@jit.edu.cn

H. Pang
School of Chemistry and Chemical Engineering
Yangzhou University
Yangzhou, Jiangsu 225009, China

M. Zhang
Key Laboratory for Photonic and Electronic Bandgap Materials
Ministry of Education
School of Physics and Electronic Engineering
Harbin Normal University
Harbin, Heilongjiang 150025, China

J. Xu
Evercos Battery Co., LTD
Suichang, Zhejiang 323300, P. R. China

J. Yang
State Key Laboratory of Multiphase Complex Systems and Center of Mesoscience
Institute of Process Engineering
Chinese Academy of Sciences
Beijing 100190, China
E-mail: jyang@mail.ipe.ac.cn

The ORCID identification number(s) for the author(s) of this article can be found under https://doi.org/10.1002/adsu.202400041

DOI: 10.1002/adsu.202400041

 © 2024 Wiley-VCH GmbH

application in water splitting.[4] Therefore, exploiting cost-effective, earth-abundant, and high-efficiency non-Pt electrocatalysts toward HER is greatly imperative.

Recently, ruthenium (Ru) has been proposed as a promising alternative to Pt for the HER due to its lower price than Pt and favorable water dissociation property.[5] Unfortunately, the incongruous binding energy of Ru—H bond results in the strong chemical adsorption of H intermediate on the surface of Ru sites, which hampers the HER activities of metallic Ru.[6] Therefore, implementing an effective strategy for the modification of hydrogen adsorption behavior of Ru is of significance to improve the electrocatalytic HER performance. As is well-known, transition metal phosphides (TMPs) with low costs and tunable valence states have attracted widespread attention in electrocatalytic fields.[7] In particular, the relatively weak hydrogen binding energy of TMPs makes them feasible options for tailoring the adsorption action of hydrogen intermediate on the Ru centers.[8] Furthermore, it has been extensively accepted that the intimate integration of metallic Ru nanoparticles and TMPs substrate could generate a strong metal-support interaction (SMSI) effect, which effectively regulates the electronic structure, accelerates the charge transfer rate, and alters the binding energy and adsorption state of intermediates, thus leading to the enhanced electrochemical intrinsic activity.[9] In addition, vacancy engineering also represents an effective strategy to promote the electrochemical performance of electrocatalysts.[10] Such as creating P vacancies in the TMPs substrate can not only construct more catalytic active sites but also benefit the stabilization of metal nanoparticles, which significantly refrains from the unfavorable agglomeration of Ru component led by high cohesive energy and improves the atom utilization, hence dramatically boosting the electrocatalytic activity and long-term durability.[11] Combined together, the rational design of Ru nanoparticles immobilized on the TMPs substrate with numerous P vacancies would be a proof-of-concept method to tailor hydrogen adsorption property and modify the electronic configuration, accordingly realizing the high-efficiency HER performance.

Motivated by the above considerations, we herein developed an "impregnation-phosphorization" strategy to synthesize homogeneously distributed Ru nanoparticles (≈2.5 nm) anchored on the 2D CoP nanosheets (denoted as Ru/CoP hereafter). The intense interaction between Ru and CoP validly regulates the electronic structure of active centers, which effectively expedites the charge transport rate and thus improves the electronic conductivity. Density functional theory (DFT) calculations demonstrate that the construction of Ru/CoP heterostructure deliberately balances the strong adsorption capacity of Ru and weak adsorption behavior of CoP, thus resulting in moderate hydrogen adsorption energy. Moreover, the formation of P vacancies in CoP substrate could availably stabilize the metallic Ru sites and increase the accessibility of active sites. As a consequence, the resultant Ru/CoP sample with the optimal Ru content exhibits distinguished HER performance with the overpotential of 36 mV to achieve a current density of 10 mA cm^{-2} in 1.0 M KOH solution, a small Tafel slope of 73.0 mV dec^{-1} and excellent long-term durability, which is comparable with the commercial Ru/C (20 wt.%). Furthermore, a two-electrode electrolyzer equipped by Ru/CoP as cathode and commercial RuO_2 as anode manifests a cell voltage of 1.562 V at 10 mA cm^{-2} and chronoamperometric curve for at least 22 h, displaying enormous practical application potentials in the water splitting field.

2. Results and Discussion

As schematically shown in **Figure 1a**, the Ru/CoP sample was fabricated via the following three steps: 1) the homogeneous precipitation preparation of α-$Co(OH)_2$ nanosheets served as CoP substrate template and precursor; 2) the formation of Ru^{3+}-anchored $Co(OH)_2$ (denoted as $Ru^{3+}/Co(OH)_2$ hereafter) via a wet impregnation strategy; 3) the vapor phosphorization of $Co(OH)_2$ into CoP nanosheets and simultaneous thermal reduction of Ru^{3+} into Ru nanoparticles in-situ immobilized onto the CoP substrate. To be specific, α-$Co(OH)_2$ nanosheets were first synthesized according to the previously reported precipitation method.[12] Transmission electron microscopy (TEM) image, scanning electron microscopy (SEM) image, and X-ray diffraction (XRD) pattern (Figure S1, Supporting Information) certify the successful generation of $Co(OH)_2$ nanosheets product with high crystalline, smooth surface and uniform morphology. Subsequently, $Ru^{3+}/Co(OH)_2$ was obtained through the wet immersion process that a certain amount of $RuCl_3$ solution was injected into the as-prepared $Co(OH)_2$ suspension.[13] As observed from XRD pattern (Figure S2a, Supporting Information) and SEM image (Figure S2b, Supporting Information), the introduction of Ru^{3+} ions doesn't alter the original composition and lamellar morphology. In addition, corresponding energy dispersive X-ray analysis (EDX) mapping images (Figure S2c, Supporting Information) indicate that plentiful Ru^{3+} ions homogeneously distribute on the surface of $Co(OH)_2$ nanosheets. Finally, Ru/CoP nanosheets were synthesized through a vapor phosphorization treatment by using sodium hypophosphite (NaH_2PO_2) as the phosphorous source. During the low-temperature phosphorization process, $Co(OH)_2$ nanosheets could react with the PH_3 gases produced from the thermal decomposition of NaH_2PO_2 to form CoP nanosheets and Ru^{3+} ions are synchronously thermally reduced to be metallic Ru nanoparticles in-situ anchored on the CoP substrate. For comparison, various samples with different Ru loading contents are also fabricated under identical synthetic conditions by varying in the concentrations of $RuCl_3$ solution (2, 3, 4, and 5 mmol L^{-1}) during the synthetic process of $Ru^{3+}/Co(OH)_2$. The resultant samples are named as Ru/CoP-2, Ru/CoP-3, Ru/CoP-4, and Ru/CoP-5, respectively. Based on the inductively coupled plasma atomic emission spectrometer (ICP-AES) results (Table S1, Supporting Information), the Ru/Co atomic mole ratios in the as-synthesized Ru/CoP-2, Ru/CoP-3, Ru/CoP-4, and Ru/CoP-5 samples are identified to be 6.3/93.7, 8.8/91.2, 11.5/88.5 and 13.3/86.7, respectively. The "impregnation-phosphorization" strategy herein holds great potential for large-scale production of electrocatalysts because of the low-cost raw materials, mild experimental environment, and simple operation procedures.

As depicted in SEM image (Figure 1b), the harvested Ru/CoP-4 sample maintains the lamellar-like structure of $Ru^{3+}/Co(OH)_2$ precursors. Nevertheless, the surface of Ru/CoP-4 product becomes slightly rough as compared with other contrastive samples. Analogously, pristine CoP, Ru/CoP-2, Ru/CoP-3, and Ru/CoP-5 also demonstrate the sheet-like morphology, as shown in Figure S3 (Supporting Information). TEM image (Figure 1c)

© 2024 Wiley-VCH GmbH

23667486, 2025, 11, Downloaded from https://advanced.onlinelibrary.wiley.com/doi/10.1002/adsu.202400041 by University Of Sao Paulo - Brazil, Wiley Online Library on [26/10/2026]. See the Terms and Conditions (https://onlinelibrary.wiley.com/terms-and-conditions) on Wiley Online Library for rules of use; OA articles are governed by the applicable Creative Commons License

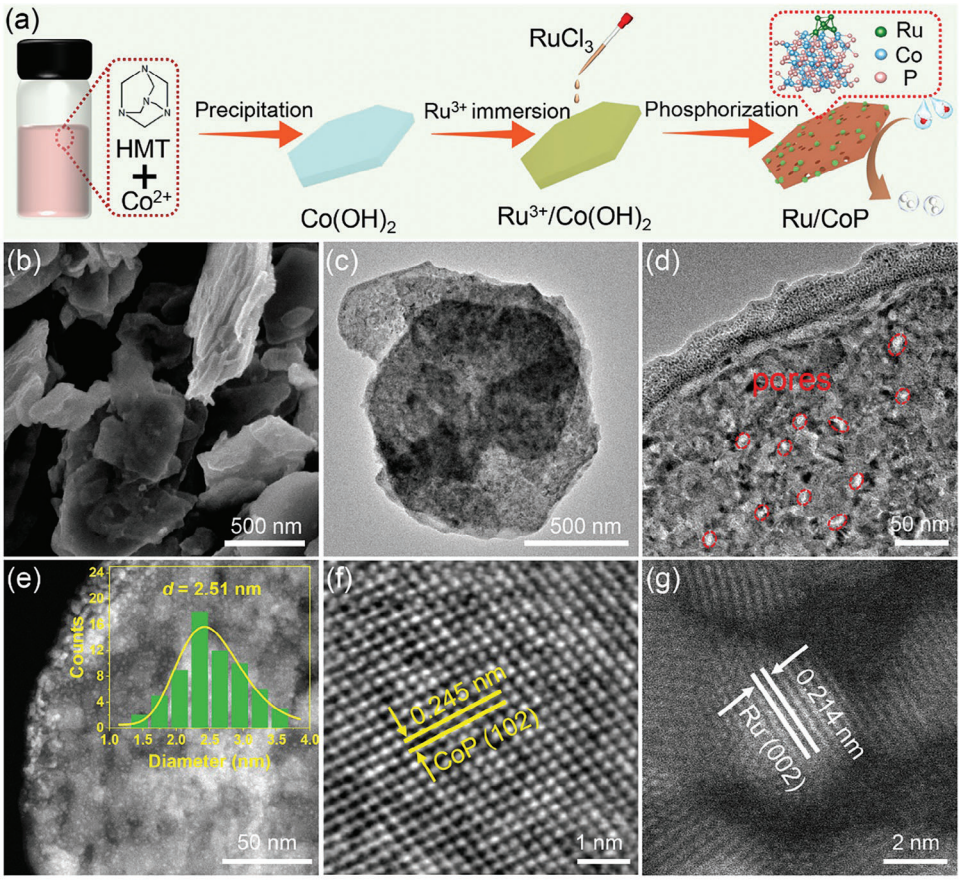

Figure 1. a) Schematic illustration for the preparation of Ru/CoP. b) SEM image, c,d) TEM images, e) AC HAADF-STEM image, and f–g) HRTEM images of the resultant Ru/CoP-4 sample.

further affirms the thin and regular nanosheet morphology of Ru/CoP-4. The magnified TEM image (Figure 1d) indicates the existence of nanopores on the CoP nanosheets, which may be led by the decomposition and gas bubbles liberation of $Co(OH)_2$ precursors. These pores on the CoP substrate are beneficial to the mass transport and electrolyte permeation during electrolysis process. As revealed by the aberration-corrected high-angle annular dark-field scanning transmission electron microscopy (AC HAADF-STEM) image (Figure 1e), numerous Ru nanoparticles with an average diameter of 2.51 nm homogeneously distribute on the surface of CoP substrate. These ultrasmall nanoparticles possess prominent advantages in electrocatalysis, such as high atomic utilization and quantum confinement effect.[14] Furthermore, as shown in the high-resolution TEM (HRTEM) images (Figure S4, Supporting Information), plentiful of Ru nanoparticles are also uniformly dispersed on the surface of CoP in Ru/CoP-2, Ru/CoP-3, and Ru/CoP-5 samples. The HRTEM image of Ru/CoP-4 (Figure 1f) demonstrates the well-resolved lattice fringes with a fringe spacing of 0.245 nm, which is in accordance with the (102) plane of orthorhombic CoP. In addition, as shown in Figure 1g, the well-resolved lattice fringe of 0.214 nm can be attributed to the (002) plane of hexagonal Ru, further testifying to the dispersion of Ru nanoparticles on the surface of CoP nanosheets. As exhibited in the HAADF-STEM and EDX mapping images (Figure S5, Supporting Information), Ru, Co, and P elements are uniformly distributed over the entire Ru/CoP sample.

As demonstrated in the XRD pattern (**Figure 2**a), all the diffraction peaks at 31.6°, 36.3°, 46.2°, 48.1°, 52.3°and 56.8° are ascribed to the (011), (111), (112), (211), (103) and (301) planes of the orthorhombic CoP, respectively.[15] Whereas, no diffraction peaks of metallic Ru can be observed herein, which may be due to its weak crystallinity and low loading amount. It is noteworthy that all the XRD patterns of the Ru/CoP family samples and CoP sample (Figure S6, Supporting Information) match well with the crystal structure of orthorhombic CoP. The surface chemistry and valence state of Ru/CoP-4 catalyst were investigated by X-ray photoelectron spectroscopy (XPS) measurement. The XPS survey spectrum of Ru/CoP-4 (Figure S7, Supporting Information) indicates the coexistence of Ru, Co, P, and C elements in the catalyst. As exhibited in Figure 2b, the high-resolution Ru 3p region of Ru/CoP-4 can be deconvoluted into four peaks, in which two main peaks located at 461.5 and 483.5 eV correspond to metallic Ru $2p_{3/2}$ and Ru $2p_{1/2}$ peaks, respectively. In addition, the other two peaks centered at 463.4 and 486.5 eV belong to Ru^{n+} $2p_{3/2}$ and Ru^{n+} $2p_{1/2}$ peaks, respectively.[16] Notably, in comparison to the commercial Ru/C (20 wt.%) composed of Ru nanoparticles anchored on carbon substrate (Figure S8, Supporting Information), all the peaks of Ru/CoP-4 prominently negatively shift to lower binding energy region. Figure 2c displays the high-resolution Co 2p spectra of

© 2024 Wiley-VCH GmbH

23667486, 2025, 11, Downloaded from https://advanced.onlinelibrary.wiley.com/doi/10.1002/adsu.202400041 by University Of Sao Paulo - Brazil, Wiley Online Library on [26/10/2026]. See the Terms and Conditions (https://onlinelibrary.wiley.com/terms-and-conditions) on Wiley Online Library for rules of use; OA articles are governed by the applicable Creative Commons License

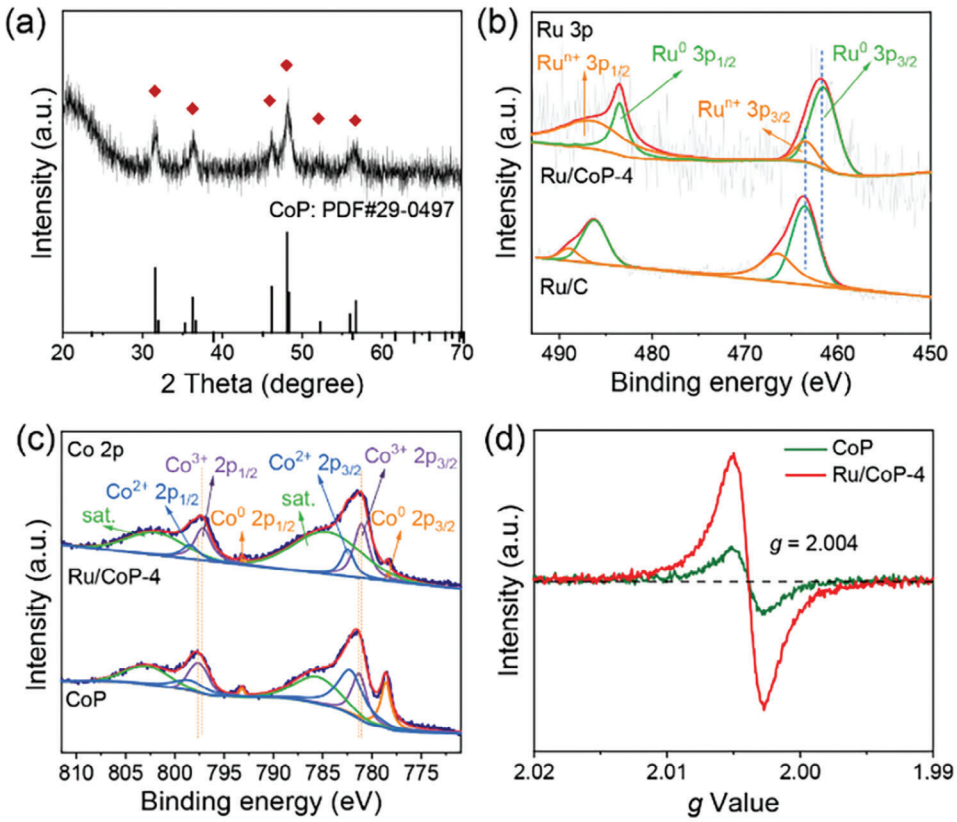

Figure 2. a) XRD pattern, b) Ru 3p XPS spectrum, c) Co 2p XPS spectrum, and d) EPR spectrum of the harvested Ru/CoP-4 product.

Ru/CoP-4 and CoP samples. Two peaks of the Ru/CoP-4 sample located at 778.4 and 793.2 eV are assigned to metallic Co $2p_{3/2}$ and Co $2p_{1/2}$, respectively. Furthermore, two pairs of deconvoluted peaks at 781.1 and 782.5 eV, and 797.2 and 798.5 eV are attributed to Co^{3+} $2p_{3/2}$ and Co^{2+} $2p_{3/2}$, and Co^{3+} $2p_{1/2}$ and Co^{2+} $2p_{1/2}$ peaks, respectively.[17] Similarly, the binding energies of Co 2p peaks in Ru/CoP-4 become lower as compared with that of pristine CoP. These above results reflect the electron transfer between Ru nanoclusters and CoP nanosheet substrate due to the SMSI effect. Moreover, an electron paramagnetic resonance (EPR) test was carried out to identify the existence of P vacancies in Ru/CoP-4 sample, as shown in Figure 2d. Obviously, Ru/CoP-4 sample possesses intensive signal intensity at a *g* value of 2.004 as compared with pristine CoP, indicating that Ru anchoring makes a positive contribution to the generation of P vacancies.[18] The formed P vacancies with rich electrons in Ru/CoP-4 catalysts not only expose more HER active sites and enhance the electronic conductivity but also stabilize the Ru nanoparticles during the electrochemical process, which benefits the improvement of HER activity and guarantees mechanical robustness.[19]

Encouraged by the SMSI effect of Ru nanoparticles and CoP substrate, the HER performances of Ru/CoP family samples were evaluated by using a typical three-electrode configuration in a 1.0 M N_2-saturated KOH electrolyte. For comparison, pristine CoP, commercial Ru/C (20 wt.%), and commercial Pt/C (20 wt.%) were also measured under identical conditions. The linear sweep voltammetry (LSV) curves with *iR*-correction are shown in **Figure** 3a. Unquestionably, commercial Pt/C exhibits the best HER performance with the smallest overpotential of 28 mV at 10 mA cm^{-2}. It is noteworthy that Ru/CoP family samples demonstrate lower overpotentials and larger current densities than pristine CoP, and the HER activities of Ru/CoP family samples are availably influenced by the Ru loading content. Specifically, as displayed in Figure 3b, Ru/CoP-4 possesses the optimal HER performance with a small overpotential of 36 mV to afford a current density of 10 mA cm^{-2}, which is lower than those of Ru/CoP-2 (81 mV), Ru/CoP-3 (44 mV), Ru/CoP-5 (72 mV) and pristine CoP (115 mV), and even exceeds that of commercial Ru/C (96 mV). The HER kinetics and mechanism of electrocatalysts were determined by Tafel slope derived from LSV curve. As illustrated in Figure 3c, the Tafel slope of Ru/CoP-4 is identified to be 73.0 mV dec^{-1}, which is lower than those of Ru/CoP-2 (77.5 mV dec^{-1}), Ru/CoP-3 (76.3 mV dec^{-1}), Ru/CoP-5 (78.3 mV dec^{-1}), CoP (90.3 mV dec^{-1}) and commercial Ru/C (79.3 mV dec^{-1}). This result demonstrates that Ru/CoP-4 sample possesses a faster reaction kinetics and the HER process that occurred on Ru/CoP-4 may follow a typical Volmer-Heyrovsky mechanism with an electrochemical desorption of chemisorbed H species as the rate-determining step.[20] Considering the small overpotential and low Tafel slope, the HER performance of Ru/CoP-4 exceeds most of the recently reported Ru-based electrocatalysts, as listed in Table S2 (Supporting Information).

The electrochemical activity of electrocatalyst was further evaluated by the electrochemical active surface area (ECSA) and electrochemical impedance spectroscopy (EIS) measurements. The ECSAs of electrocatalysts are linearly proportional to their

© 2024 Wiley-VCH GmbH

23667486, 2025, 1, Downloaded from https://advanced.onlinelibrary.wiley.com/doi/10.1002/adsu.202400041 by University Of Sao Paulo - Brazil, Wiley Online Library on [26/10/2026]. See the Terms and Conditions (https://onlinelibrary.wiley.com/terms-and-conditions) on Wiley Online Library for rules of use; OA articles are governed by the applicable Creative Commons License

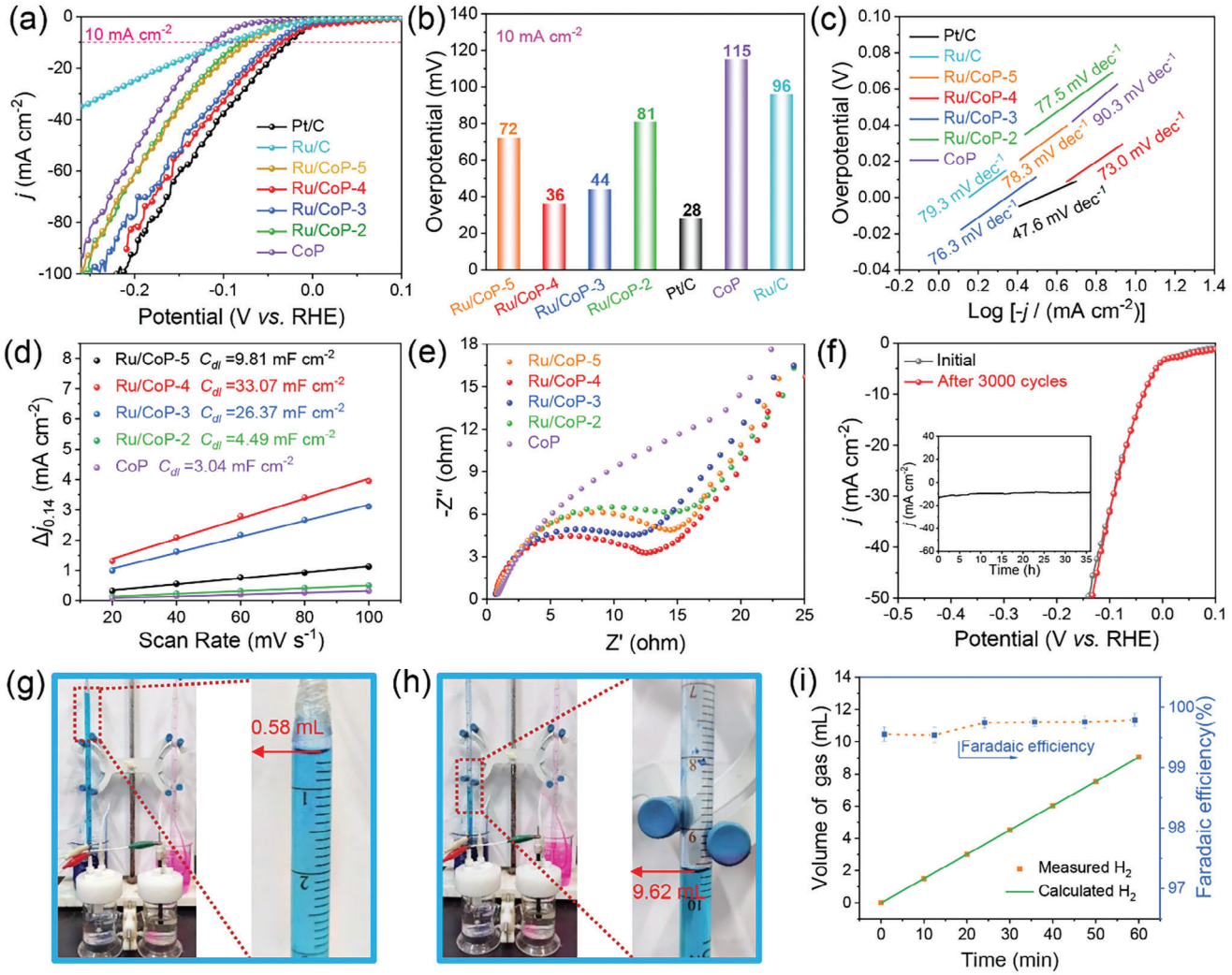

Figure 3. Electrocatalytic HER performance of different catalysts in 1.0 M KOH electrolyte. a) LSV polarization curves, b) overpotentials at 10 mA cm^{-2}, c) Tafel plots, d) C_{dl} values, e) Nyquist plots tested at −1.106 V, f) LSV curves of Ru/CoP-4 electrocatalyst before and after 3000-cycle CV test. (Inset of panel f: the chronopotentiometry curve at a constant overpotential of 70 mV). g,h) Digital photographs of two-electrode electrolyzers before and after electrolysis, i) experimental and theoretical yields of H_2 gas and Faradaic efficiency of the Ru/CoP-4 sample during water splitting process at 20 mA cm^{-2} for 1 h. The error bars represent standard deviations from three independent measurements.

double-layer capacitance (C_{dl}), which can be determined by cyclic voltammetry (CV) curves with different scan rates at non-faradaic potential ranges (Figure S9, Supporting Information).[21] As exhibited in Figure 3d, the C_{dl} values of Ru/CoP-2, Ru/CoP-3, Ru/CoP-4, Ru/CoP-5, and pristine CoP electrocatalysts are calculated to be 4.49, 26.37, 33.07, 9.81 and 3.04 mF cm^{-2}, respectively, indicating more exposure of active sites in the optimal Ru/CoP-4 sample. According to the Nyquist plots (Figure 3e), Ru/CoP-4 sample possesses the smallest charge transfer resistance (R_{ct}) as compared with the other Ru/CoP family samples and pristine CoP sample, suggesting the fastest charge transfer rate during HER process.[22] Given the similar structural features of Ru/CoP samples, it can be reasonably postulated that the appropriate ratio of Ru and CoP could generate the optimal regulation effect for electronic structure and H intermediate adsorption. Besides the electrochemical activity, the long-term stability represents the other vital parameter to evaluate the electrocatalytic performance of electrocatalysts.[23] As shown in Figure 3f, the almost overlapped LSV curves before and after 3000 CV cycles demonstrate the excellent stability of Ru/CoP-4. Furthermore, the steady amperometric *i–t* curve for 24 h with negligible decay (inset of Figure 3f) for 36 h at a constant overpotential of 70 mV further confirms the prominent electrochemical durability of Ru/CoP sample. In addition, SEM and TEM measurements were employed to analyze the architectural stability of Ru/CoP-4 product after HER durability test. As observed from the SEM image (Figure S10a, Supporting Information) and TEM images (Figure S10b,c, Supporting Information), the Ru/CoP sample still maintains the morphology composed of Ru nanoparticles immobilized on CoP nanosheet after 3000 cycle CV test, implying its outstanding structural robustness. Furthermore, the water drainage method was carried out to estimate the faradaic efficiency of H_2 evolution (Figure 3g,h). As shown in Figure 3i, the obtained gas volume-time curve indicates that the volume of

© 2024 Wiley-VCH GmbH

23667486, 2025, 11, Downloaded from https://advanced.onlinelibrary.wiley.com/doi/10.1002/adsu.202400041 by University Of Sao Paulo - Brazil, Wiley Online Library on [26/10/2026]. See the Terms and Conditions (https://onlinelibrary.wiley.com/terms-and-conditions) on Wiley Online Library for rules of use; OA articles are governed by the applicable Creative Commons License

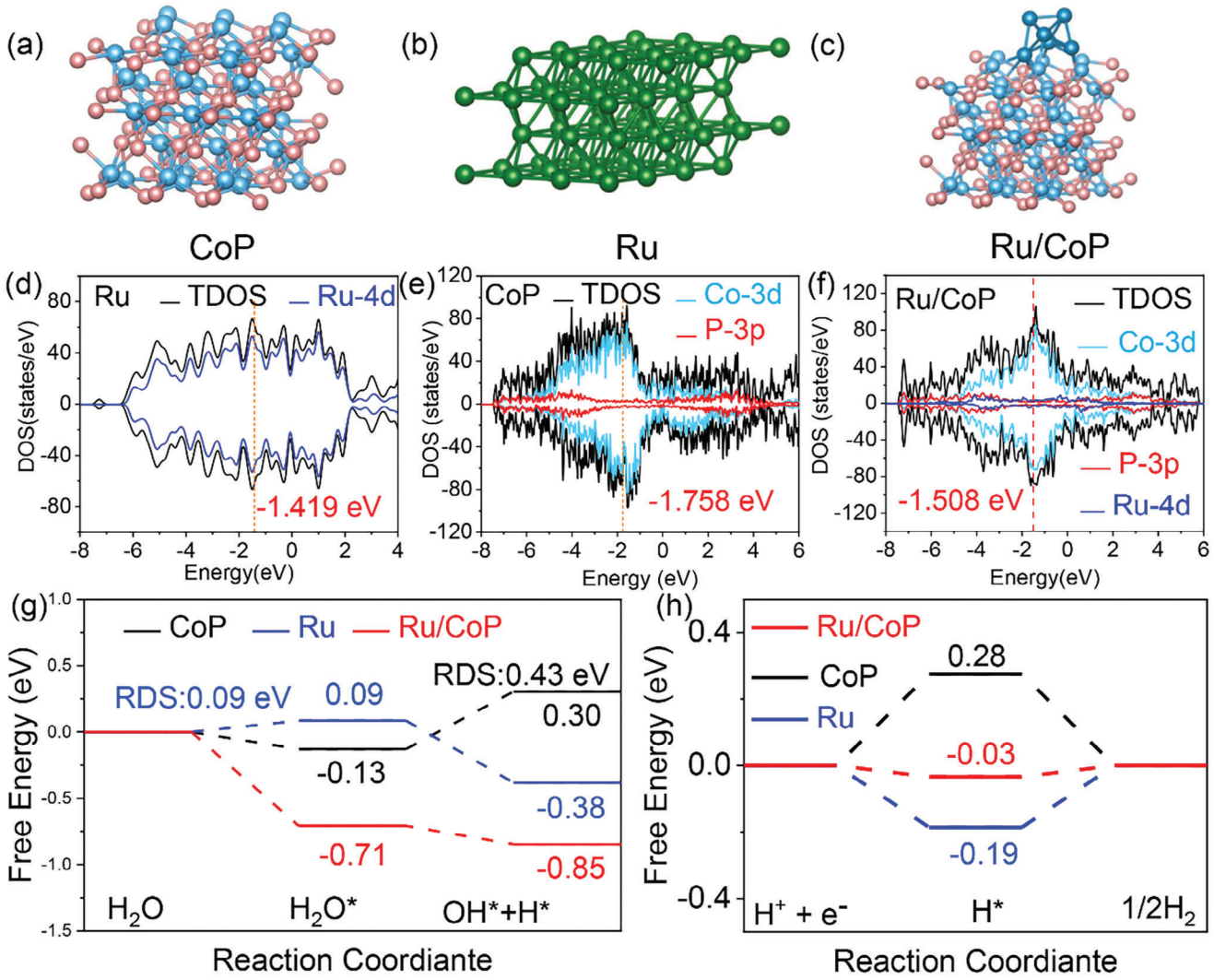

Figure 4. The models of a) pristine CoP, b) pristine Ru, and c) Ru/CoP. d–f) DOSs distributions of pristine Ru, pristine CoP, and Ru/CoP, g) H_2O adsorption and dissociation energies, and h) ΔG_{H^*} diagrams of pristine Ru, pristine CoP, and Ru/CoP.

generated H_2 gas volume coincides with the calculated yield, reflecting that the Faraday efficiency of HER process is close to 100%.

To deeply understand the contribution of SMSI between Ru and CoP for the improved HER activity, density functional theory (DFT) calculations were executed to uncover the reaction mechanisms of Ru/CoP. **Figure** 4a–c exhibits the computational models of pristine Ru, pristine CoP, and Ru/CoP, respectively. As demonstrated in electronic density of state (DOS) diagrams (Figure 4d–f), the d-band center of Ru/CoP is in between the pristine Ru and pristine CoP, reflecting that the formation of Ru/CoP structure neutralizes the strong adsorption strength of Ru and weak adsorption ability of CoP. This moderate adsorption strength could availably prevent the toxification of the electrocatalyst caused by the difficult adsorption of reactant and hard desorption of product, thus benefiting the occurrence of HER.[24] Figure S11 (Supporting Information) displays the optimized theoretical models of H_2O^*, OH*+H*, and H* on the surfaces of pristine Ru, pristine CoP and Ru/CoP. As for the adsorption and dissociation processes of H_2O (Figure 4g), Ru/CoP possesses the most excellent adsorption capacity for H_2O molecular as compared with pristine CoP and pristine Ru, and the followed dissociation process of H_2O is a spontaneous process. However, the Gibbs adsorption energies of H_2O molecular on the surface of pristine Ru is determined to be 0.09 eV, reflecting a non-spontaneous process for the adsorption of H_2O. Furthermore, the activated dissociation energy barrier of H_2O for pristine CoP is calculated to be 0.43 eV, which also represents a non-spontaneous process. These results reflect the favorable activated dissociation ability of water on Ru/CoP. As observed from the Gibbs free energy of H adsorption (ΔG_{H^*}) diagrams (Figure 4h), the ΔG_{H^*} values of pristine CoP and pristine Ru are 0.28 and −0.19 eV, respectively, indicating the rate-determining steps (RDS) of pristine CoP and pristine Ru are adsorption of H* and desorption of $1/2H_2$, respectively. Notably, the ΔG_{H^*} value of Ru/CoP is −0.03 eV, which is close to the ideal HER activity. This result can be attributed to the strong interfacial electron interaction between Ru and CoP overcomes the inappropriate adsorption problems of Ru and CoP, and

© 2024 Wiley-VCH GmbH

23667486, 2025, 11, Downloaded from https://advanced.onlinelibrary.wiley.com/doi/10.1002/adsu.202400041 by University Of Sao Paulo - Brazil, Wiley Online Library on [26/10/2026]. See the Terms and Conditions (https://onlinelibrary.wiley.com/terms-and-conditions) on Wiley Online Library for rules of use; OA articles are governed by the applicable Creative Commons License

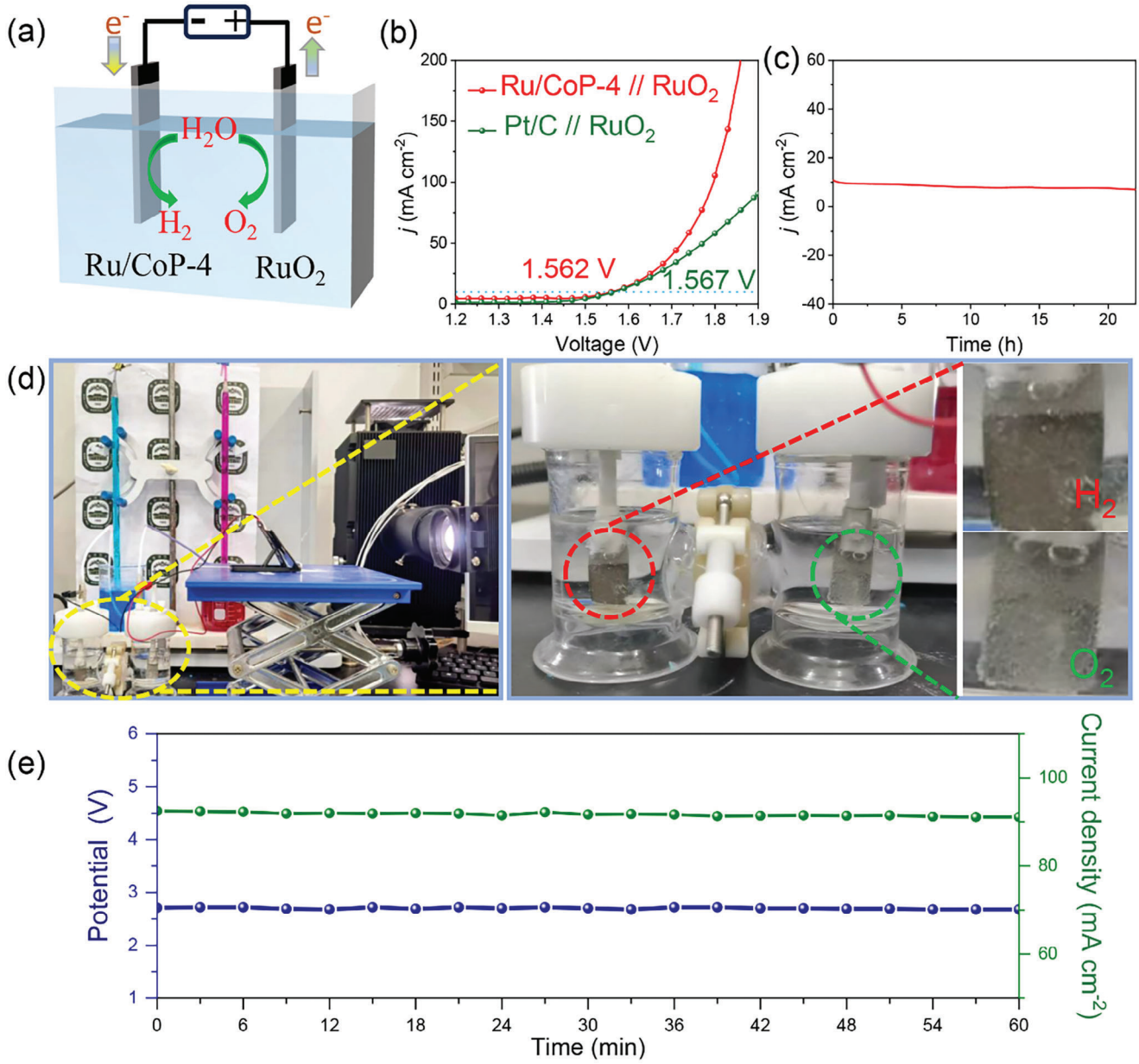

Figure 5. The overall water splitting performance of Ru/CoP-4//RuO_2 electrolyzer. a) The model, b) LSV curves, c) the chronopotentiometry curve at a cell voltage of 1.65 V. d) Digital photograph of a solar energy-driven H-type electrolyzer assembled by Ru/CoP-4 and RuO_2, and e) the voltage and generated current density of the solar cell during the daytime for water splitting.

correspondingly makes Ru/CoP suitable adsorption and desorption strengths. In a word, the above DFT results undoubtedly confirm that the construction of Ru/CoP structure contributes to the modification of H adsorption state, thereby leading to enhanced HER performance.

In view of the excellent HER performance of Ru/CoP-4 electrocatalyst, a two-electrode electrolyzer by using Ru/CoP-4 as cathode and commercial RuO_2 as anode (denoted as Ru/CoP-4//RuO_2 hereafter, **Figure** 5a) was constructed to appraise the practicability in water electrolysis field. For comparison, a water-splitting device assembled by commercial Pt/C (20 wt.%) as cathode and commercial RuO_2 as anode (denoted as Pt/C//RuO_2 hereafter) was chosen as benchmark. As displayed in Figure 5b, Ru/CoP-4//RuO_2-assembled electrolyzer requires a low cell voltage of 1.562 V to afford a current density of 10 mA cm^{-2}, which is on a par with that of Pt/C//RuO_2 reference (1.567 V) and surpass many recently reported non-Pt-based electrocatalysts (Table S3, Supporting Information). What's more, as observed from the *i–t* curve (Figure 5c), the water electrolytic cell can retain the steady current density over 22 h at an applied voltage of 1.65 V, suggesting the remarkable stability of Ru/CoP-4//RuO_2-assembled electrolyzer. Furthermore, an H-type electrolyzer separated with an anion-exchange membrane driven by electricity converted form solar energy (Figure 5d) was built to further evaluate the

© 2024 Wiley-VCH GmbH

23667486, 2025, 11, Downloaded from https://advanced.onlinelibrary.wiley.com/doi/10.1002/adsu.202400041 by University Of Sao Paulo - Brazil, Wiley Online Library on [26/10/2026]. See the Terms and Conditions (https://onlinelibrary.wiley.com/terms-and-conditions) on Wiley Online Library for rules of use; OA articles are governed by the applicable Creative Commons License

practicability of Ru/CoP-4 electrocatalyst in water electrolysis. Obviously, a mass of H_2 and O_2 gas bubbles can be noticed from the cathode and anode respectively in Figure 5d. Notably, the solar cell could generate a voltage of ≈2.7 V and provide corresponding current density of nearly 91 mA cm^{-2} (Figure 5e) at different reaction times for 1 h. The above results unquestionably prove that the Ru/CoP-4 electrocatalyst holds extremely applicable value in the water electrolytic process.

3. Conclusion

In conclusion, we have presented a facile approach to synthesize the ultrafine Ru nanoparticles in situ grown on the surface of CoP nanosheet substrate for high-performance hydrogen evolution. The SMSI effect between Ru nanoparticles and CoP nanosheets could effectively facilitate the water-activated dissociation energy and modify the hydrogen adsorption ability of Ru/CoP electrocatalyst, which is beneficial for the improved electrochemical HER process. In addition, the creation of P vacancies can guarantee the firm contact of Ru and CoP substrate and concurrently endow the Ru/CoP products with numerous active sites and enhanced electronic conductivity. As a consequence, the harvested Ru/CoP-4 sample with optimal Ru loading content exhibits impressive HER performance in an alkaline medium, with a low overpotential of 36 mV at a current density of 10 mA cm^{-2}, a small Tafel slope of 73.0 mV dec^{-1}, and outstanding long-term durability for 36 h, which is comparable to the commercial Pt/C benchmark. This concept of tailored hydrogen adsorption state by SMSI effect would open an effective approach for future electrocatalysts in water-splitting fields.

Supporting Information

Supporting Information is available from the Wiley Online Library or from the author.

Acknowledgements

Y.Z. and J.L. contributed equally to this work. This work was supported by the National Natural Science Foundation of China (22272179, 22072067, 22232004).

Conflict of Interest

The authors declare no conflict of interest.

Data Availability Statement

Research data are not shared.

Keywords

hydrogen adsorption behavior, hydrogen evolution reaction, Ru nanoparticles, strong metal-support interaction

Received: January 16, 2024
Revised: February 28, 2024
Published online: March 15, 2024

[1] a) F. Zhang, Y. Liu, F. Yu, H. Pang, X. Zhou, D. Li, W. Ma, Q. Zhou, Y. Mo, H. Zhou, *ACS Nano* **2023**, *17*, 1681; b) Q. Zhou, R. Sun, Y. Ren, R. Tian, J. Yang, H. Pang, K. Huang, X. Tian, L. Xu, Y. Tang, *Carbon Energy* **2023**, *5*, e273; c) J. Zhang, C. Ma, S. Jia, Y. Gu, D. Sun, Y. Tang, H. Sun, *Adv. Energy Mater.* **2023**, *13*, 2302436; d) Z. Wu, B. Liu, H. Jing, H. Gao, B. He, X. Xia, W. Lei, Q. Hao, *J. Colloid. Interf. Sci.* **2023**, *629*, 22. e) M. S. A. Sher Shah, G. Y. Jang, K. Zhang, J. H. Park, *EcoEnergy* **2023**, *1*, 344; f) Y. Song, W. Xie, M. Shao, X. Duan, *Nano Mater. Sci.* **2023**, *5*, 161.

[2] a) L. K. Putri, B. J. Ng, R. Y. Z. Yeo, W. J. Ong, A. R. Mohamed, S. P. Chai, *Chem. Eng. J.* **2023**, *461*, 141845; b) T. Cui, J. Chi, J. Zhu, X. Sun, J. Lai, Z. Li, L. Wang, *Appl. Catal. B: Environ* **2022**, *319*, 121950; c) J. Su, J. Zhou, L. Wang, C. Liu, Y. Chen, *Sci. Bull.* **2017**, *62*, 633; d) S. Zhang, X. Zhou, G. Zhou, B. He, H. Pang, L. Xu, Y. Tang, *Chem. - Eur. J.* **2023**, *29*, e202301252; e) Z. Wu, Q. Li, G. Xu, W. Jin, W. Xiao, Z. Li, T. Ma, S. Feng, L. Wang, *Adv. Mater.* **2023**, 2311018; f) P. Yang, F. Liu, X. Zang, L. Xin, W. Xiao, G. Xu, H. Li, Z. Li, T. Ma, J. Wang, Z. Wu, L. Wang, *Adv. Energy Mater.* **2023**, 2303384.

[3] a) Y. Zeng, M. Zhao, Z. Huang, W. Zhu, J. Zheng, Q. Jiang, Z. Wang, H. Liang, *Adv. Energy Mater.* **2022**, *12*, 2201713; b) G. Zhou, C. Wei, Z. Li, B. He, Z. Liu, J. Li, *Inorg. Chem. Front.* **2024**, *11*, 164; c) J. Li, Z. Xia, Q. Xue, M. Zhang, S. Zhang, H. Xiao, Y. Ma, Y. Qu, *Small* **2021**, *17*, 2103018; d) Y. N. Zhou, W. L. Yu, H. J. Liu, R. Y. Fan, G. Q. Han, B. Dong, Y. M. Chai, *EcoEnergy* **2023**, *1*, 425; e) G. Liu, Y. Xu, T. Yang, L. Jiang, *Nano Mater. Sci.* **2023**, *5*, 101.

[4] a) H. Song, M. Wu, Z. Tang, J. S. Tse, B. Yang, S. Lu, *Angew. Chem., Int. Ed.* **2021**, *60*, 7234; b) J. Xu, C. Chen, X. Kong, *Nano Energy* **2023**, *111*, 108403; c) Q. Liang, Q. Li, L. Xie, H. Zeng, S. Zhou, Y. Huang, M. Yan, X. Zhang, T. Liu, J. Zeng, K. Liang, O. Terasaki, D. Zhao, L. Jiang, B. Kong, *ACS Nano* **2022**, *16*, 7993; d) Z. Wu, P. Yang, Q. Li, W. Xiao, Z. Li, G. Xu, F. Liu, B. Jia, T. Ma, S. Feng, L. Wang, *Angew. Chem., Int. Ed.* **2023**, *62*, e202300406; e) Z. Chen, Q. Li, H. Xiang, Y. Wang, P. Yang, C. Dai, H. Zhang, W. Xiao, Z. Wu, L. Wang, *Inorg. Chem. Front.* **2023**, *10*, 1493.

[5] J. T. Ren, L. Chen, H. Y. Wang, W. W. Tian, X. Zhang, T. Y. Ma, Z. Zhou, Z. Y. Yuan, *Appl. Catal. B: Environ* **2023**, *327*, 122466.

[6] Y. Yang, Y. Yu, J. Li, Q. Chen, Y. Du, P. Rao, R. Li, C. Jia, Z. Kang, P. Deng, Y. Shen, X. Tian, *Nano-Micro Lett.* **2021**, *13*, 160.

[7] a) X. Huang, X. Xu, C. Li, D. Wu, D. Cheng, D. Cao, *Adv. Energy Mater.* **2019**, *9*, 1803970; b) Y. R. Hao, H. Xue, J. Sun, N. Guo, T. Song, J. Sun, Q. Wang, *ACS Appl. Mater. Interfaces* **2021**, *13*, 56035; c) Z. Lu, Y. Cao, J. Xie, J. Hu, K. Wang, D. Jia, *Chem. Eng. J.* **2022**, *430*, 132877; d) H. Song, J. Yu, Z. Tang, B. Yang, S. Lu, *Adv. Energy Mater.* **2022**, *12*, 2102573.

[8] J. Li, Z. Jing, H. Bai, Z. Chen, A. I. Osman, M. Farghali, D. W. Rooney, P. S. Yap, *Environ. Chem. Lett.* **2023**, *21*, 2583.

[9] a) C. Li, S. H. Kim, H. Y. Lim, Q. Sun, Y. Jiang, H. J. Noh, S. J. Kim, J. Baek, S. K. Kwak, J. B. Baek, *Adv. Mater.* **2023**, *35*, 2301369; b) X. Wang, X. Yang, G. Pei, J. Yang, J. Liu, F. Zhao, F. Jin, W. Jiang, H. Ben, L. Zhang, *Carbon Energy* **2023**, e391.

[10] a) Y. Zhang, R. Lu, C. Wang, Y. Zhao, L. Qi, *Adv. Funct. Mater.* **2023**, *33*, 2303073; b) W. Ding, S. Yuan, Y. Yang, X. Li, M. Luo, *J. Mater. Chem. A* **2023**, *11*, 23653; c) Z. Wu, Y. Zhao, W. Jin, B. Jia, J. Wang, T. Ma, *Adv. Funct. Mater.* **2021**, *31*, 2009070; d) T. Guo, H. Fei, R. Liu, F. Liu, D. Wang, Z. Wu, *Appl. Catal. B: Environ* **2024**, *343*, 123480.

[11] a) J. Zhu, J. Chi, T. Cui, L. Guo, S. Wu, B. Li, J. Lai, L. Wang, *Appl. Catal. B: Environ.* **2023**, *328*, 122487; b) J. Duan, S. Chen, C. A. Ortiz-Ledon, M. Jaroniec, S. Z. Qiao, *Angew. Chem., Int. Ed.* **2020**, *59*, 8181; c) X. Wang, X. Liu, S. Wu, K. Liu, X. Meng, B. Li, J. Lai, L. Wang, S. Feng, *Nano Energy* **2023**, *109*, 108292; d) H. Huang, K. Liu, F. Yang, J. Cai, S. Wang, W. Chen, Q. Wang, L. Fu, Z. Xie, S. Xie, *Angew. Chem., Int. Ed.* **2023**, *62*, e202315752.

 © 2024 Wiley-VCH GmbH

23667486, 2025, 11, Downloaded from https://advanced.onlinelibrary.wiley.com/doi/10.1002/adsu.202400041 by University Of Sao Paulo - Brazil, Wiley Online Library on [26/10/2026]. See the Terms and Conditions (https://onlinelibrary.wiley.com/terms-and-conditions) on Wiley Online Library for rules of use; OA articles are governed by the applicable Creative Commons License

[12] G. Zhou, M. Li, Y. Li, H. Dong, D. Sun, X. Liu, L. Xu, Z. Tian, Y. Tang, *Adv. Funct. Mater.* **2020**, *30*, 1905252.
[13] J. Zhang, X. Xu, L. Yang, D. Cheng, D. Cao, *Small Methods* **2019**, *3*,1900653.
[14] J. Wang, X. Guan, H. Li, S. Zeng, R. Li, Q. Yao, H. Chen, Y. Zheng, K. Qu, *Nano Energy* **2022**, *100*, 107467.
[15] C. Yuan, T. Xu, M. Guo, Y. Sun, T. Zhang, X. Yu, *Appl. Catal. B: Environ* **2024**, *343*, 123562.
[16] Z. Jiang, S. Song, X. Zheng, X. Liang, Z. Li, H. Gu, Z. Li, Y. Wang, S. Liu, W. Chen, D. Wang, Y. Li, *J. Am. Chem. Soc.* **2022**, *144*, 19619.
[17] a) Z. Wang, K. Chi, S. Yang, J. Xiao, F. Xiao, X. Zhao, S. Wang, *Small* **2023**, *198*, 2301403; b) T. Liu, P. Li, N. Yao, G. Cheng, S. Chen, W. Luo, Y. Yin, *Angew. Chem., Int. Ed.* **2019**, *131*, 4727; c) L. Yang, X. Cao, X. Wang, Q. Wang, L. Jiao, *Appl. Catal. B: Environ* **2023**, *329*, 122551.
[18] X. Liu, Q. Yu, X. Qu, X. Wang, J. Chi, L. Wang, *Adv. Mater.* **2024**, *36*, 2307395.
[19] R. Sun, Y. Bai, Z. Bai, L. Peng, M. Luo, M. Qu, Y. Gao, Z. Wang, W. Sun, K. Sun, *Adv. Energy Mater.* **2022**, *12*, 2102739.
[20] a) J. Zhao, J. Wang, X. Zheng, H. Wang, J. Zhang, J. Ding, X. Han, Y. Deng, W. Hu, *Small Methods* **2023**, *7*, e2201362; b) H. Li, M. Zhang, L. Yi, Y. Liu, K. Chen, P. Shao, Z. Wen, *Appl. Catal. B: Environ* **2021**, *280*, 119412.
[21] J. Li, C. Hou, C. Chen, W. Ma, Q. Li, L. Hu, X. Lv, J. Dang, *ACS Nano* **2023**, *17*, 10947.
[22] P. K. L. Tran, D. T. Tran, M. Austeria P, D. H. Kim, N. H. Kim, J. H. Lee, *Adv. Energy Mater.* **2023**, *13*, 2203844.
[23] S. Wang, X. Ning, X. Liu, M. Shakouri, Y. Hu, H. Yuan, P. Liu, X. Lu, Y. Guo, Y. Wang, *Carbon* **2024**, *217*, 118611.
[24] G. Zhou, S. Zhang, Y. Zhu, J. Li, K. Sun, H. Pang, M. Zhang, Y. Tang, L. Xu, *Small* **2023**, *19*, 2206781.

© 2024 Wiley-VCH GmbH

23667486, 2025, 11, Downloaded from https://advanced.onlinelibrary.wiley.com/doi/10.1002/adsu.202400941 by University Of Sao Paulo - Brazil, Wiley Online Library on [26/10/2026]. See the Terms and Conditions (https://onlinelibrary.wiley.com/terms-and-conditions) on Wiley Online Library for rules of use; OA articles are governed by the applicable Creative Commons License